Geologica Acta, Vol.11, Nº 1, March 2013, 103-112
DOI: 10.1344/105.000001760
Available online at www.geologica-acta.com

geologica acta

Origin of superimposed and curved slickenlines in San Miguelito range, Central México

S. XU A.F. NIETO-SAMANIEGO S.A. ALANIZ-ÁLVAREZ

Universidad Nacional Autónoma de México
Centro de Geociencias, Apartado Postal 1-742, Querétaro, Qro., 76001, México. Xu E-mail: sxu@dragon.geociencias.unam.mx

ABSTRACT

Interactions between intersecting faults cause local perturbations of the stress field in the vicinity of their intersections. Fault intersections are places of stress accumulation, stress relief and refraction of the stress trajectories; the slip vectors near these intersections are deviated from the maximum shear stress resolved by the far-field stress. In an intersecting fault system, superimposed, arc-shaped and zigzag slickenlines can be formed due to interaction between intersecting faults. We propose some mechanisms in which it is possible to recognize that the superimposed and curved slickenlines are produced from curvilinear translational fault motion. The geometrical models presented in this contribution are consistent with the slickenlines distribution observed in the vicinity of intersection lines, measured in the San Miguelito range, Mesa Central, México. Two tectonic phases have been inferred from our slip vector models near the intersection lines, which is consistent with observations of previously published work.

KEYWORDS | **Superimposed slickenlines. Curved slickenlines. Fault interaction. San Miguelito. México.**

INTRODUCTION

Intersecting faults are commonly observed at different scales. For two intersecting faults, the fault that inhibits the movement of the other is described as the restricting fault. The other one is described as the restricted fault (Fig. 1). The restricted fault can be formed before, after or coeval to the restricting fault. Secondary faults are commonly restricted by the primary faults. They are formed in the regions of fault tips, jogs, and other geometric irregularities of the primary fault (*e.g.* Kim and Sanderson, 2006). Conjugate faults are formed in the same tectonic phase and cut each other, forming a rhombic fault system in two dimensions. Newly formed faults can both cut the older faults and be restricted by the pre-existing faults or weakness planes.

Because movement on one fault is inhibited by the other intersecting fault, their intersections form locked areas where stress concentration occurs. In this way, fault intersections could be the places of big earthquake occurrence (*e.g.* Talwani 1999). For example, geologists observe locally curved shapes of spreading axes, normal fault scarps, and abyssal hills, when they approach the transform faults (Morgan and Parmentier, 1984; Blackman and Forsyth, 1989; Sonder and Pockalny, 1999). The given explanation for these observations is that the least compressive stress changes progressively in orientation and increases in magnitude near the ridge-transform intersection (Morgan and Parmentier, 1984). Stephansson *et al.* (1991) propose that the application of a far-field global stress state to a faulted crust will result in stress

concentrations, stress relief and refraction of the stress trajectories in the vicinity of fault intersections. Peltzer *et al.* (2001) show that the inferred slip rate on a conjugate fault system in the Eastern California shear zone is three times greater than its long-term slip rate estimated from geological data. Multiple slickenline sets, which are not consistent with tensor solutions on the fault planes, could be produced under the same far-field stress (*e.g.* Cashman and Ellis, 1994; Nieto-Samaniego and Alaniz-Alvarez, 1997). In this contribution we propose that some superimposed and curved slickenlines are due to kinematic interaction between two intersecting faults and could be explained by using a simple geometrical model.

GEOLOGICAL BACKGROUND OF SAN MIGUELITO RANGE IN THE MESA CENTRAL, MÉXICO

The San Miguelito range in the Mesa Central, México, was chosen for testing our models because it is located in a simple geologic setting and the normal fault system is well exposed. In this way, slickenlines along the normal faults can be systematically measured.

The San Miguelito range is a relatively uplifted area of the southern Mesa Central physiographic province located in central México (Fig. 2A). It is constituted by a large amount of silicic volcanic rocks of Oligocene age (*e.g.* Nieto-Samaniego *et al*., 1996), which overlay the Mesozoic marine rocks of the Sierra Madre Oriental fold and thrust belt. The Oligocene volcanic sequence is formed by five main units (Labarthe-Hernández and Jiménez-López, 1992). This Oligocene volcanism was controlled by a history of mostly extensional tectonic events (Labarthe-Hernández and Jiménez-López, 1992). The large axes and the alignment of volcanic domes commonly indicate the orientations of large normal faults (Xu *et al.*, 2008). From bottom to top, the main units are: Portezuelo Latite and rhyodacite, San Miguelito Rhyolite, Cantera Ignimbrite, Zapote Rhyolite, Panalillo Ignimbrite (Fig. 2C). The first unit has a reported age of 30.6±1.5Ma (K-Ar, whole rock) by Labarthe-Hernández *et al.* (1982); for the last unit, an isotopic date of 27.6±0.6Ma (K-Ar, sanidine) was reported by Labarthe-Hernández and Jiménez-López (1992). Two volcanic cycles are distinguished. The first one is a lava bed including the Portezuelo Latite and rhyodacite and the San Miguelito Rhyolite. The second one is mainly an ignimbrite bed with intercalated rhyolite and basalt, represented by the Cantera Ignimbrite, Zapote Rhyolite, Panalillo Ignimbrite (Torres-Hernández *et al.*, 2001, 2006).

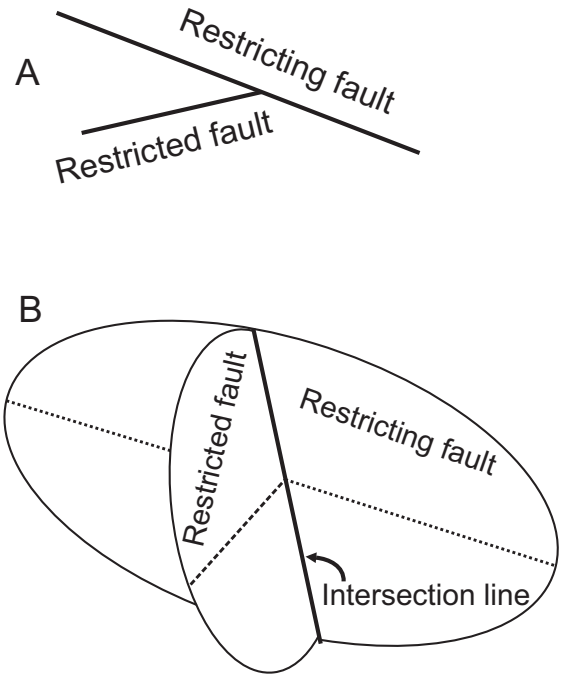

FIGURE 1 | Intersecting fault system showing the restricting and restricted faults mentioned in the text. A) In two dimensions; B) In three dimensions.

The San Miguelito range is bounded by the Villa de Reyes NE-SW Graben and is part of the San Luis -Tepehuanes NW-SE fault system (Nieto-Samaniego *et al.*, 1999, 2005). Individual faults within the range have a strike direction of 300º-340º and dip to the SW (Fig. 2B). The beds are tilted to the NE systematically with dip angles between 12º and 31º. The fault system exhibits a "domino style geometry" as the faults are sub-parallel and the beds systematically tilt to the NE (Labarthe-Hernández and Jiménez-López, 1992; Xu *et al.*, 2004).

OBSERVED SLICKENLINES

In the field, the pitches of slickenlines were measured by using the right-hand rule. Pitch is measured from the right-hand side of the fault strike to the slickenlines. In this work, two areas for detailed observation of slickenlines are shown in Figure 2D and E. Although the movement of faults inferred from displacements of stratigraphic units is normal, the pitches measured in this study range from 0º to 180º. Previous work shows that the pitches of most normal faults in the studied area are not equal to 90º (Xu *et al.*, 2004).

The superimposed slickenlines shown in Figures 3 and 4 were observed along fault 1 marked in Figure 2E and on the plane of fault B marked in Figure 2D, respectively. New slickenlines commonly cut old ones. In this way, the older slickenlines are covered by the new ones and appear off and on. When the older slickenlines are not worn completely,

they appear unclearly. For these systems of superimposed slickenlines, two types are distinguished. The first type is the system in which the pitch of older slickenlines (P1) is larger than that of younger ones (P2) that means P2-P1<0. Most of the pitch patterns belong to this type (Fig. 3A, B, C, F, G; Table 1). The other type includes the system in which the pitch of older slickenlines is less than that of younger ones, that is to say, P2-P1>0 (Fig. 3D; Table 1). The variation of pitch for all superimposed slickenlines is from 42° to 120°. The angles between older and younger slickenlines vary from 25° to 78°. The methods of paleostress inversion are based on the assumption that the maximum shear stress vector resolved on the plane is parallel to the slickenlines on the fault plane (*e.g.* Angelier, 1994; Etchecopar *et al.*, 1981; Zalohar and Vrabec, 2010). In other words, the slickenlines on a fault indicate the direction of the traction vector along the fault plane. The slickenlines can be divided into four groups according to their angle of pitch when it is less than 90° (Fig. 5A). Similarly, when the angle of pitch is from 90° to 180°, another four groups can be obtained. In the study area, all eight groups of slickenlines are observed (Fig. 5B). The large change of slickenlines should be interpreted as produced by inhomogeneities in the stress field, multiple tectonic phases or fault interaction. In the study area, a possible interpretation of the observed multiple slickenside

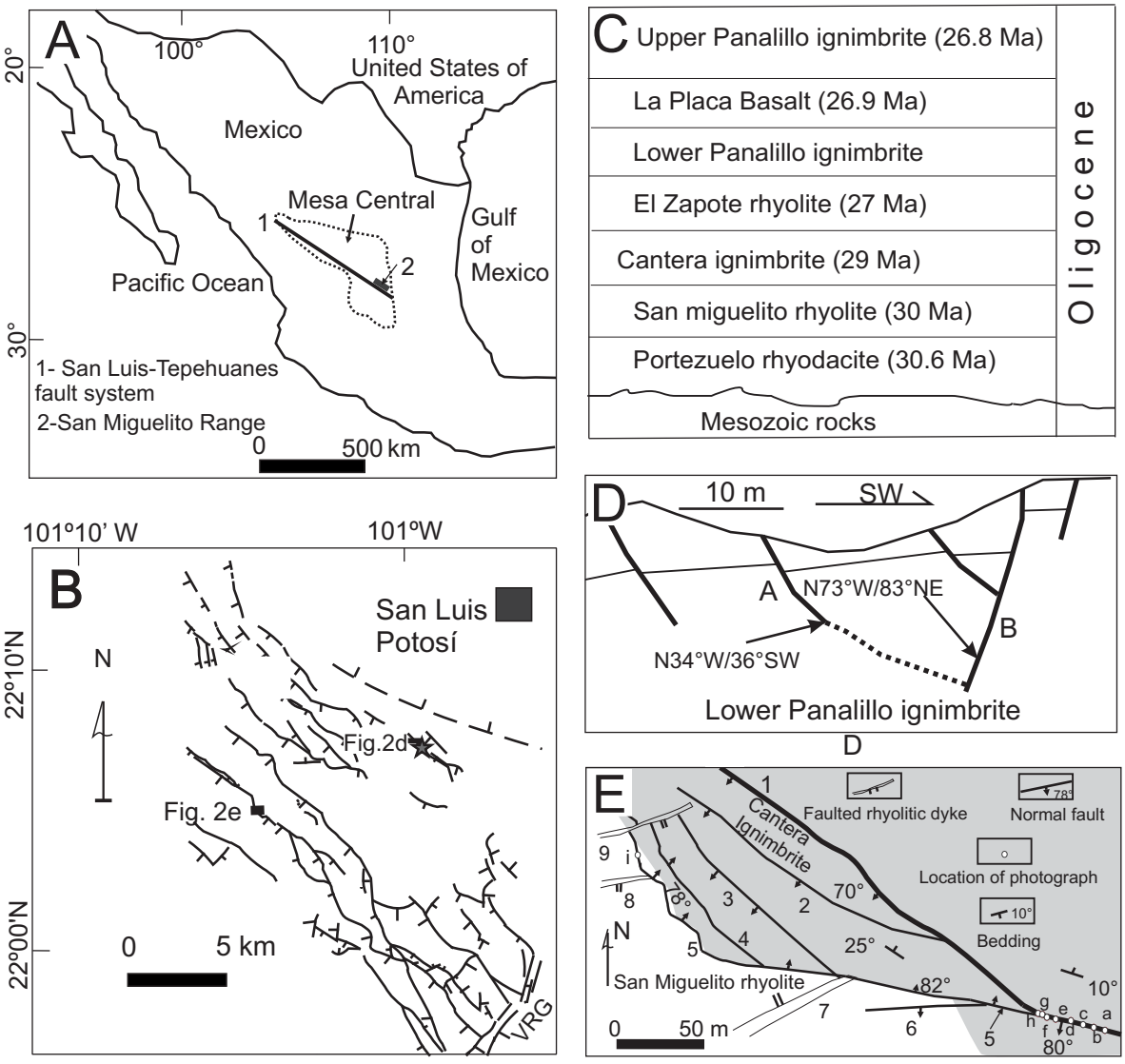

FIGURE 2 | A) Location of Mesa Central and the San Miguelito range. B) Distribution of normal faults in San Miguelito range in the Mesa Central, México. VGR: Villa de Reyes Graben. C) Stratigraphic column and ages for the San Miguelito range (from Torres-Hernández et al., 2006). D) Field section showing intersecting faults whose location is shown in B. E) Intersecting normal fault system observed from the area indicated in B.

groups is that multiple tectonic phases took place during the development of the normal faults. However, according to Nieto-Samaniego *et al.* (2005), the faults of the San Miguelito range are part of the San Luis-Tepehuanes fault system, for which only two tectonic phases are documented. In this way, the observed superimposed slickenlines cannot be explained only by different tectonic phases, and it is necessary to consider other mechanisms. Based on these considerations, we analyze the variation in slip direction due to mechanical interaction between the faults with intersecting patterns.

Curved slickenlines are observed on the plane of fault 1 (Fig. 3C, E, H; Fig. 4A, B). There are two types of curved slickenlines. One type of curved slickenlines is curved clockwise and has rightward convexity (Figs. 3C, E, 4B). The initial pitch of slickenlines (P1) is smaller than the final pitch (P2) for this type of curved slickenlines (Table 1). The other curves are counterclockwise and display leftward convexity, for which the beginning pitch of slickenlines (P1) is larger than the ending pitch (P2) for this type of curved slickenlines (Figs. 3H, 4A; Table 1). Previously, the curved slickenlines are widely documented (*e.g.* Tricart *et al.*, 2004). Kusky *et al.* (1997) proposed that the curved slickenlines may be resulted from progressive exhumation of the Chugach accretionary wedge in Alaska while the faults were active. Theoretically, the curved slickenlines can be explained either due to rotational-translational fault motion or due to curvilinear fault motion where the translation direction changes continuously (Mandal and Chakraborty, 1989; Twiss and Gefell, 1990; Twiss and Unruh, 2007). In our examples, the most curved slickenlines in the assemblage are of identical shape, which is the characteristic of curvilinear fault motion (Mandal and Chakraborty, 1989). On the other hand, because the dips of faults on which the slickenlines are observed are larger than 80º (Fig. 2D, E), little rotation for these restricting faults (fault 1 in Fig. 2E and fault B in Fig. 2D) occurred during activity. Then, the curved

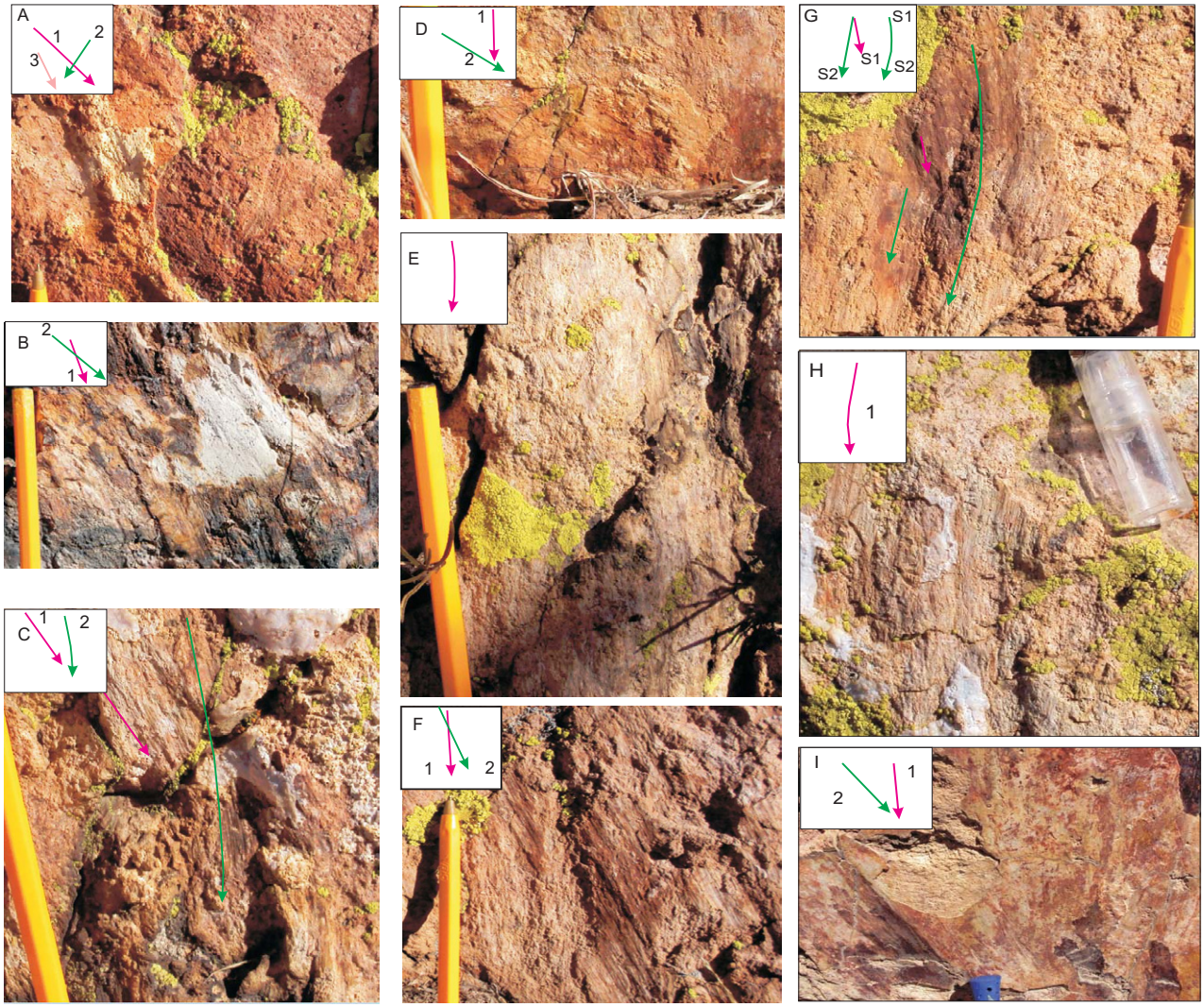

FIGURE 3 | Superimposed and curved slickenlines taken from fault 5 with the lens to the northeast. Locations of photographs are indicated in Figure 2E. Labels S1, S2 and numbers are for identification of the equivalent slickenlines in models of Figure 6.

slickenlines should have been produced by continuous changes in translation direction. One good example in Figure 3G displays that the curved and superimposed slickenlines can be observed in the same position. On the left in Figure 3G, S1 and S2 are superimposed, whereas on the right, there are transitional slickenlines between S1 and S2, their combination forms curved slickenlines. Our data indicate that if the angle between the beginning pitch and ending pitch of slickenlines (a) is less than 20º (Fig. 3E, H; Fig. 4A-B), curved slickenlines tend to be formed. When the value of a is from 20º to 25º, both superimposed and curved slickenlines can be formed (*e.g.* Fig. 3G). When the value of a is larger than 25º, superimposed slickenlines can be formed.

EXPLANATIONS TO THE FORMATION OF SUPERIMPOSED AND SINUOUS SLICKENLINES

In intersecting fault systems, the slickenside orientation near intersection lines generally does not coincide with

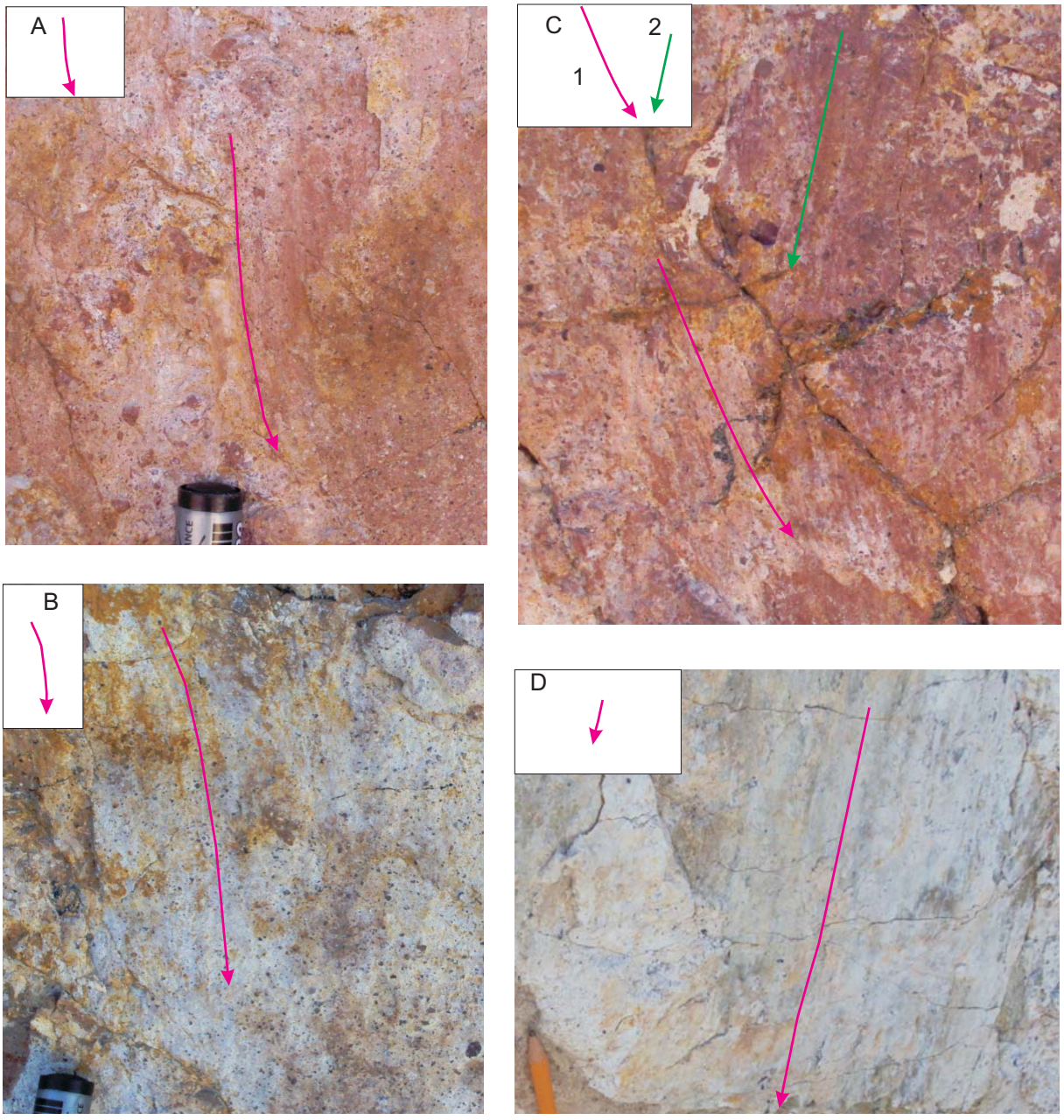

FIGURE 4 | Slickenline patterns taken from the plane of fault B in Fig. 2D with the lens facing southwest. The location of photographs is indicated by the star in Figure 2B. The numbers (1,2) are for identification of the equivalent slickenlines in the models of Figure 7.

TABLE 1 | Pitch angles for the superimposed and curved slickenlines shown in Figure 3 and Figure 4. For the superimposed slickenlines, P1 is the pitch of older ones, and P2 is the pitch of younger ones. For the curved slickenlines, P1 is the pitch of the initial tangent of the curve, and P2, the pitch of the end tangent of the curve

	Fig. 3A	Fig. 3B	Fig. 3C	Fig. 3D	Fig. 3E	Fig. 3F	Fig. 3G	Fig. 3H	Fig. 3I	Fig. 4A	Fig. 4B
P1	42°	70°	57°	86°	80°	87°	81°	95°	93°	88°	68°
P2	120°	41°	84°	150°	93°	62°	104°	86°	129°	70°	84°
P2-P1	78°	-29°	27°	53°	13°	-25°	23°	-9°	36°	-18°	16°

the direction of the maximum shear stress resolved by the remote stress tensor. This is documented by fieldwork (*e.g.* Mouslopoulou *et al.*, 2008) and by some numerical models based on linear elasticity theory (Dupin *et al.*, 1993; Pollard *et al.*, 1993; Maerten, 2000). An angle discrepancy (q) between the slip direction on the fault plane and the direction of resolved shear stress is also predicted from their models. There are two tendencies of the slip vectors in the vicinity of the intersections in restricting normal faults (Maerten, 2000; Nieto-Samaniego and Alaniz-Alvarez, 1997). One is that the slip vectors tend to be parallel to the intersection line, whereas the other is that the slip vectors tend to be perpendicular to the intersection line. According to the results of Dupin *et al.* (1993), the range of the modeling slip directions reaches 47º for intersecting faults. Pollard *et al.* (1993) obtain that the largest discrepancy due to fault interaction is 37º. On the other hand, Maerten's results indicate that the discrepancy of slip vectors due to fault interaction is more than 50º. In general, the discrepancy is dependent upon Poisson's ratio, the angle between the strikes of the intersecting faults, and fault aspect ratio (Pollard *et al.*, 1993; Maerten, 2000). It is also documented that the angle discrepancy of slip vectors on the restricted fault is commonly larger than that on the restricting fault (Pollard *et al.*, 1993; Maerten, 2000). Then, the slickenlines on the restricted fault can be parallel to the intersection line. Especially Nieto-Samaniego and Alaniz-Alvarez (1997) proposed that the slickenlines on the restricted fault should be parallel to the intersection line. We only discuss the slickenlines on the restricting fault in this paper.

Based on results of numerical models mentioned above, we propose a possible origin of superimposed and curved slickenlines due to fault interaction. Figure 6 explains the slickenlines shown in Figure 3 which were observed from fault 1 in Figure 2E. For the intersecting system in Figure 2E, fault 1 is a restricting fault and fault 5 is a restricted fault. The stereoplot indicates that the intersection line on fault 1 has a pitch of less than 90º (Fig. 6A). The distribution of slip vectors of the hanging wall on the restricting fault is shown in Figure 6B, in which the resolved shear stress far from the intersection line has a pitch of 90º. One can see that, on the hanging wall side (left part) of the restricted fault (fault 5), the slip vectors on the restricting fault (fault 1) tend to be parallel to the inclined intersection line, and the pitch of slip vectors is less than 90º. However, on the footwall side of the restricted fault (right part), the slip vectors on the restricting fault become more perpendicular to the intersection line and the pitch of slip vectors is larger than 90°. The perturbation of slip vectors is larger near the fault intersection. Figure 6C and D show the formation of superimposed slickenlines. In Figure 6C, when the intersection line is located in position 1, area A is on the hanging wall side of the restricted fault. As a result, the pitch of slickenlines S1 is larger than 90º. With the continuous movement of the fault system in a tectonic phase, the intersection line is moved to the left and

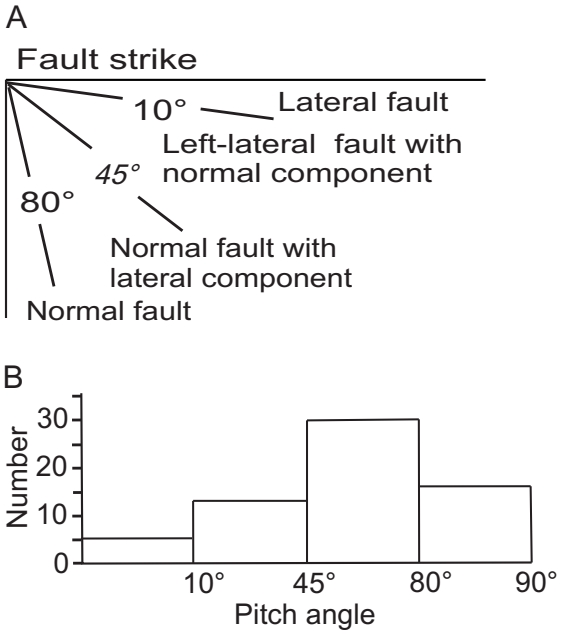

FIGURE 5 | A) Classification of the pitch angle of fault slickenlines for P < 90º. B) Histogram of the pitch angle of fault slickenlines observed in the study area.

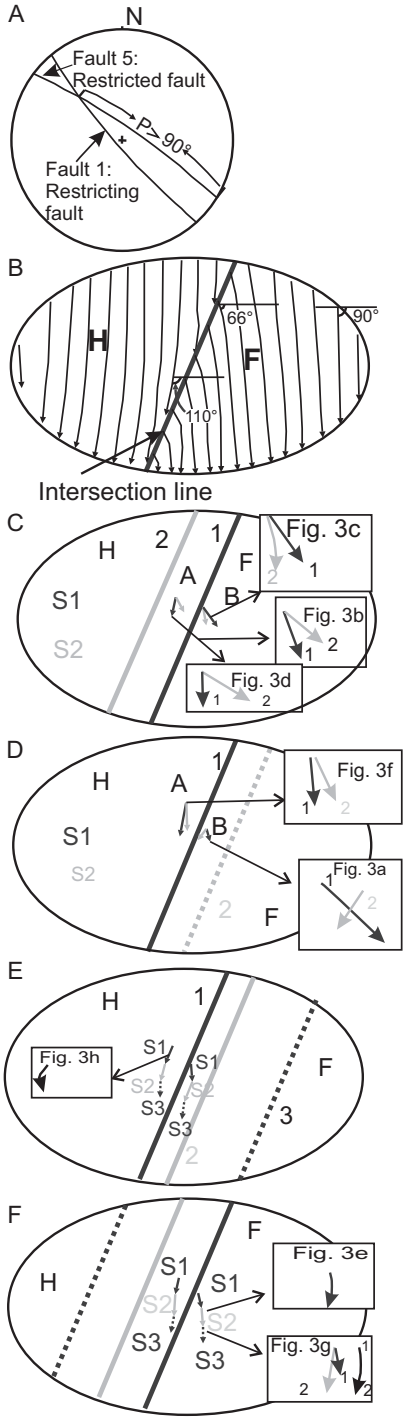

FIGURE 6 | A) Stereoplot of faults 1 and 5 shown in Figure 2E. P: pitch angle of intersection line on the restricting fault. B) Distribution of slip vectors on the restricting fault in the intersecting fault system (modified from Maerten, 2000). H: Hanging wall of restricted fault; F: Foot wall of restrictedfault. The ellipse represents the footwall of the restricting fault. C) and D) Models showing the formation of arc-shape and zigzag slikenlines. According to slip distribution in (B) when the intersection line moves to E) right and F) to left (see detailed explanation in text). Numbers (1,2,3) refer to steps in the deformation sequence. Labels S1, S2 and S3 indicate the slikenlines fomed during each step.

is located in position 2, then, the new set of slickenlines S2 are formed and superimposed on S1. Now area A is on the footwall side of the restricted fault. Then, the pitch of S2 is less than 90º. In this area, the pitch of older slickenlines (S1) is larger than that of younger ones (S2). The pitch of S1 is less than 90º and the pitch of S2 is larger than 90º. The slickenlines in Figure 3B and D are similar to the patterns in area A. On the other hand, the evolution of the slip vector in area B is different from that in area A. In this area, the pitch of older slickenlines (S1) is smaller than that of younger ones (S2). Both pitch angles are less than 90º. The slickenlines in Figure 3C are consistent with the slip vectors in area B.

In Figure 6D, the movement direction of the intersection line is the opposite of that in Figure 6C. Over time in a tectonic phase, a new intersection line is located to the right of the previous intersection line. Then, the superimposed slickenlines are different from those in Figure 6C. In area A, the pitch of old slickenlines (S1) is larger than that of new ones. The superimposed slickenlines in Figure 3F can represent the slip vectors in area A. In area B, the pitch of old slickenlines (S1) is less than that of new ones (S2). The superimposed slickenlines in Figure 3A indicate the slip pattern in area B.

On the other hand, formation of curved slickenlines is explained in Figure 6E and F. Figure 6E shows that the intersection line is moved rightward. The slickenlines S1, S2 and S3 are formed as the intersection line is in positions 1, 2, and 3, respectively. On the left of the intersection line, the pitch of slickenlines becomes increasingly smaller. In this way, S1, S2 and S3 show a leftward convex curve. The variable range of the pitch for the curve will be dependent on the amount of movement from the intersection line, the angle between the strikes of the intersecting faults and the stress ratio. Slickenlines in Figure 3H coincide with this slip pattern. On the right of the intersection line, the pitch of S2 is larger than that of S1, whereas the pitch of S3 is smaller than that of S2. In this way, the sets of slickenlines S1, S2, and S3 form a zigzag curve or anti-S-shaped curve. If combining the beginning and the end of the slickenlines of 1, 2 and 3 in Figure 3A, we can obtain a zigzag curve like that on the right of Figure 6E. The intersection line in Figure 6F is moved to the left. As a result, on the right of the intersection line, the pitch of slickenlines becomes progressively large. In this way, S1, S2 and S3 form a rightward convex curve. Slickenlines in Figure 3E are consistent with this curve pattern. On the left of the intersection line, the pitch of S2 is less than that of S1, whereas the pitch of S3 is larger than that of S2. Then, the sets of slickenlines S1, S2, and S3 show a S-shaped curve.

Also, we give a model (Fig. 7) to explain the intersecting fault system in Figure 2D and the curved slickenlines in Figure 4. The intersection line on the restricting fault (fault

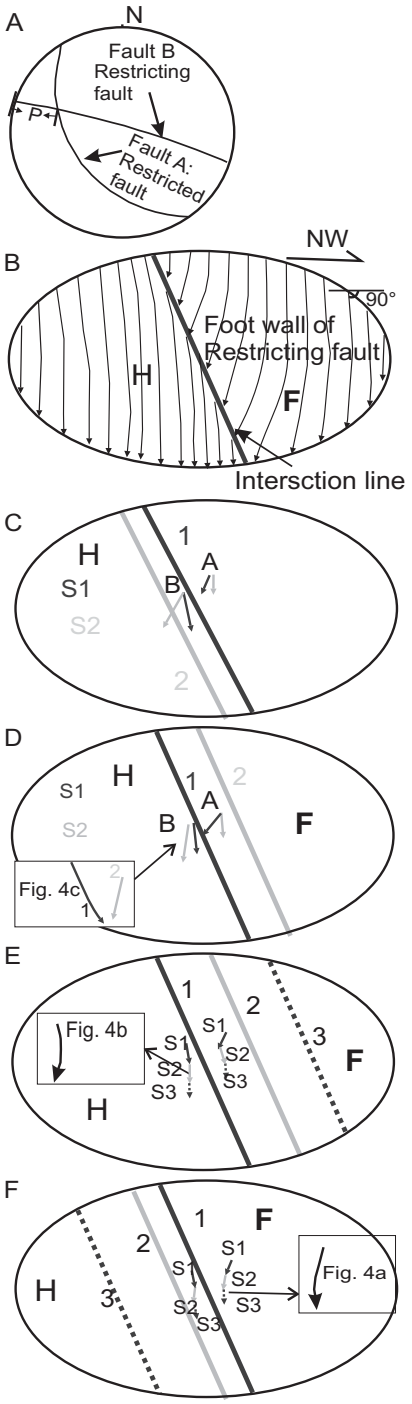

FIGURE 7 | A) Stereoplot of faults A and B shown in Figure 2D. P: pitch angle of intersection line on restricting fault. B) Distribution of slip vectors on the restricting fault in the intersecting fault zone (Modified from Maerten, 2000). H: Hanging wall of restricted fault; F: Foot wall of restricted fault. C) and D) Models showing the formation of superimposed slickenlines based on the slip pattern shown in B when the intersection line moves C) leftward or D) rightward. E) and F) Model explaining the formation of arc-shape and zigzag slickenlines according to slip distribution in B when the intersection line moves to E) the right and to F) the left (see detailed explanation in text). Numbers (1,2,3) refer to steps in the deformation sequence. Labels S1, S2 and S3 indicate the slikenlines fomed during each step.

B) has a pitch less than 90º (Fig. 7A, B). On the left part of the intersection line, the slip vectors tend to be parallel to the intersection line, and the pitch of slip vectors is less than 90º. On the right part of the intersection line, the slip vectors tend to be perpendicular to the intersection line, and the pitch of slip vectors is larger than 90º. Based on the distribution of slip vectors, we obtain two superimposed slickenline models and two curved slickenline models (Fig. 7C, D, E, F). One photograph of superimposed slickenlines was observed (Fig. 4C) and two types of curved slickenlines were obtained (Fig. 4A, B). The superposed slickenlines represent the case of Figure 7D. The two curved slickenlines are consistent with the cases in Figure 7E and F, respectively.

In general, the cases in Figures 6 and 7 shows that most superimposed slickenlines in the San Miguelito range should be produced by interaction in intersecting faults. Also, the two examples show that two directions of movement occurred for the restricted faults in Figures 6 and 7. In Figure 6, we can see that the leftward movement of the restricted fault is represented by the slickenline patterns in Figure 3B, C, D, E, F and Figure 4G, and rightward movement of the restricted fault is represented by that in Figure 3A, F, H. Similarly to Figure 7, the slickenline pattern in Figure 4A indicates the leftward movement of the restricted fault, and those in 4B, C show the rightward movement of the restricted fault. Based on these observations, we consider that at least there were two tectonic phases which produced different displacements on faults: one phase produced leftward movement of intersection lines, and the other, caused rightward movement of the intersection line. The pitches of the curved slickenlines are 65º-95º (Table 1), which indicate that the normal faults for two tectonic phases are nearly pure normal faults. This is consistent with previous observations in the Mesa Central (*e.g.*, Nieto-Samaniego *et al.*, 1999, 2005).

Patterns 3A, B and D in Figure 6 require that the slickenlines on the restricting fault surface must pass from one side to the other of the fault intersection. According to Xu *et al.* (2004), the heave of fault 1 in Figure 2E is 75m, the fault dips are from 64º to 80º, and the pitches of slickenlines vary from 42º to 95º. If the median values of fault dip (72°) and pitch angle (68°) are used, the calculated strike displacement is 90m. Considering this horizontal displacement of 90m, the present location of the intersection and the distance between the first point "a" and the intersection line is about 45m, it is possible that observed points have been moved from one side to another of the intersection.

CONCLUSIONS

Superimposed and curved slickenlines associated with intersecting fault arrays were documented in the

San Miguelito range of Mesa Central, México. The angle between superimposed slickenlines varies from 25º to 78º, whereas the variation of the curved slickenlines is from 9° to 21°. The pitch angle of new superimposed slickenlines can be larger than or less than that of old ones, depending on the position and distance from the intersection line. Also, the curved (arc-shaped and zigzag) slickenlines can occur in the vicinity of the intersecting line between the two fault planes. Whether arc-shaped or zigzag slickenlines are formed depends on the positions where the slickenlines are located. We compare the superimposed and curved slickenlines measured in the San Miguelito range with the fault interaction model of Maerten (2000) and found that the patterns of slickenlines are well consistent with the theoretical model. The majority of the slickenlines are not parallel to the maximum shear stress vector produced by the far-field stress tensor; instead, they are better explained by stress perturbations near fault intersections.

ACKNOWLEDGMENTS

This work was supported by the 049049 and 80142 Conacyt projects of México and the project PAPIIT IN107610. We thank the kind help of Isidro Loza Aguirre and Alejandro Manzano López in the fieldwork. The helpful comments by Alfonso Muñoz-Martín and an anonymous reviewer are also appreciated.

REFERENCES

Angelier, J., 1994. Paleostress determinations. In: Hancock, P.L. (ed.). Continental Deformation. Tarrytown (New York), Pergamon Press, 53-100.

Blackman, D.K., Forsyth, D.W., 1989. Axial topographic relief associated with ridge-transform intersections. Earth and Planetary Science Letters, 95, 115-129.

Cashman, P.H., Ellis, M.A., 1994. Fault interaction may generate multiple slip vectors on a single fault surface. Geology, 22, 1123-1126.

Dupin, J-M., Sassi, W., Angelier, J., 1993. Homogeneous stress hypotheses and actual fault slip: a distinct element analysis. Journal of Structural Geology, 15, 1033-1043.

Etchecopar, A., Vasseur, G., Daignieres, M., 1981. An inverse problem in microtectonics for the determination of stress tensors from fault striation analysis. Journal of Structural Geology, 3, 51-65.

Kim, Y.S., Sanderson, D.J., 2006. Structural similarity and variety at the tips in a wide range of strike-slip faults: a review. Terra Nova, 18, 330-344.

Kusky, T.M., Bradley, D.C., Haeussler, P., 1997. Progressive deformation of the Chugach accretionary complex, Alaska, during a paleogene ridge-trench encounter. Journal of Structural Geology, 19, 139-157.

Labarthe-Hernández, G., Jiménez-López, L.S., 1992. Características físicas y estructura de lavas e ignimbritas riolíticas en la Sierra de San Miguelito. Universidad Autónoma de San Luis Potosí, Instituto Geología, Folleto técnico (Open File Report), 114, 31pp.

Labarthe-Hernández, G., Tristán-González, M., Aranda-Gómez, J.J., 1982. Revisión estratigráfica del Cenozoico de la parte central del Estado de San Luis Potosí. Universidad Autónoma de San Luis Potosí, Instituto Geología, Folleto técnico (Open File Report), 85, 208pp.

Mandal, N., Chakraborty, C., 1989. Fault motion and curved slickenlines: a theoretical analysis. Journal of Structural Geology, 11, 497-501.

Maerten, L., 2000. Variations in slip on intersecting normal faults: implications for paleostress inversion. Journal of Geophysical Research, 270, 197-206.

Morgan, J.P., Parmentier, E.M., 1984. Lithospheric stress near a ridge-transform intersection. Geophysical Research Letters, 11, 113-116.

Mouslopoulou, V., Nicol, A., Walsh, J.J., Beetham, D, Stagpoole, V., 2008. Quaternary temporal stability of a regional strike-slip and rift fault intersection. Journal of Structural Geology, 30, 451-463.

Nieto-Samaniego, Á.F., Macías-Romo, C., Alaniz-Álvarez, S.A., 1996. Nuevas edades isotópicas de la cubierta volcánica cenozoica de la parte meridional de la Mesa Central, México. Revista Mexicana de Ciencias Geologicas, 13, 117-122.

Nieto-Samaniego, Á.F., Alaniz- Álvarez, S.A., 1997. Origin and tectonic interpretation of multiple fault patterns. Tectonophysics, 270, 197-206.

Nieto-Samaniego, Á.F., Ferrari, L., Alaniz- Álvarez, S.A., Labarthe-Hernández, G., Rosas-Elguera, J., 1999. Variation of Cenozoic extension and volcanism across the southern Sierra Madre Occidental Volcanic Province, México. Geological Society of America Bulletin, 111, 347-363.

Nieto-Samaniego, Á.F., Alaniz- Álvarez, S.A., Camprubi Cano, A., 2005. La Mesa Central de México: estratigrafía, estructura y evolución tectónica cenozoica. Boletín de la Sociedad Geológica mexicana, 57, 285-317.

Peltzer, G., Crampré, F., Hensley, S., Rosen, P., 2001. Transient strain accumulation and fault interaction in the Eastern California shear zone. Geology, 29, 975-976.

Pollard, D.D., Salitzer, S.D., Rubin, A.M., 1993. Stress inversion methods: are they based on faulty assumptions? Journal of Structural Geology, 15, 1045-1054.

Sonder, L.J., Pockalny, R.A., 1999. Anomalously rotated abyssal hills along active transforms: Distributed deformation of oceanic lithosphere. Geology, 27, 1003-1006.

Stephansson, O., Ljunggren, C., Jing, L., 1991. Stress measurements and tectonic implications for Fennoscandia. Tectonophysics, 189, 317-322.

Talwani, P., 1999. Fault geometry and earthquakes in continental interiors. Tectonophysics, 305, 371-379.

Torres-Hernández, J.R., Labarthe-Hernández, G., Tristán-González, M., Aguillón-Robles, A., Siebe-Grabach, C.,

Macías-Vázquez, J.L., Espíndola-Castro, J.M., Aranda-Gómez, J.J., 2001. Vulcanismo y extensión: la evolución de un campo volcánico en el Altiplano Central de México. Instituto Nacional de Geoquímica (INAGEQ), actas, 7(1), 58pp.

Torres-Hernández, J.R., Labarthe-Hernández, G., Aguillón-Robles, A., Gómez-Anguiano, M., Mata-Segura, J.L., 2006. The pyroclastic dikes of the Tertiary San Luis Potosí volcanic field: Implications on the emplacement of Panalillo ignimbrite. Geofísica Internacional, 45, 243-253.

Tricart, P., Schwartz, S., Sue, C., Lardeaux, J., 2004. Evidence of synextension tilting and doming during final exhumation from analysis of multistage faults (Queyras Schistes lustre's, Western Alps). Journal of Structural Geology, 26, 1633-1645.

Twiss, R.J., Gefell, M.J., 1990. Curved slickenfibers: a new brittle shear sense indicator with application to a sheared serpentinite. Journal of Structural Geology, 12, 471-481.

Twiss, R.J., Unruh, J.R., 2007. Structure, deformation and strength of the Loma Prieta fault, northern California, USA, as inferred from 1989-1990 Loma Prieta aftershock sequence. Geological Society of America Bulletin, 119, 1079-1106.

Xu, S-S., Nieto-Samaniego, Á.F., Alaniz-Álvarez, S.A., 2004. Tilting mechanism in domino faults of the Sierra de San Miguelito, Central México. Geologica Acta, 2(3), 189-201.

Xu, S-S, Nieto-Samaniego, Á.F., Alaniz-Álvarez, S.A., Grajales-Nishimura, J.M., 2008. Evolution of the geometry of normal faults in the Oligocene volcanic field of the Mesa Central, México. Boletín de la Sociedad Geológica Mexicana, 60(1), 71-82.

Zalohar, J., Vrabec, M., 2010. Kinematics and dynamics of fault reactivation: The Cosserat approach. Journal of Structural Geology, 32, 15-27.

Manuscript received April 2011;
revision accepted November 2011;
published Online February 2012.